Lawrence Berkeley National Laboratory
Lawrence Berkeley National Laboratory

Title

Water adsorption, solvation and deliquescence of alkali halide thin films on SiO2 studied by ambient pressure X-ray photoelectron spectroscopy

Permalink
https://escholarship.org/uc/item/4102p5rd

Author
Arima, Kenta

Publication Date
2010-01-14

eScholarship.org
Powered by the California Digital Library
University of California

Water adsorption, solvation and deliquescence of alkali halide thin films on SiO_2 studied by ambient pressure X-ray photoelectron spectroscopy

Kenta Arima[1], Peng Jiang[2,3], Xingyi Deng[2,4], Hendrik Bluhm[5],

and Miquel Salmeron[2,3]

[1] Department of Precision Science and Technology, Graduate School of Engineering, Osaka University, 2-1, Yamada-oka, Suita, Osaka 565-0871, Japan

[2]Materials Sciences Division, Lawrence Berkeley National Laboratory, Berkeley, California 94720, USA

[3]Department of Materials Science and Engineering, University of California–Berkeley, Berkeley, California 94720, USA

[4]Parsons Project Services, Inc., National Energy Technology Laboratory, United States Department of Energy, P. O. Box 10940, Pittsburgh, Pennsylvania 15236, USA

[5]Chemical Sciences Division, Lawrence Berkeley National Laboratory, Berkeley, California 94720, USA

.

Abstract

The adsorption of water on KBr thin films evaporated onto SiO_2 was investigated as a function of relative humidity (RH) by ambient pressure X-ray photoelectron spectroscopy. At 30% RH adsorbed water reaches a coverage of approximately one monolayer. As the humidity continues to increase, the coverage of water remains constant or increases very slowly until 60% RH, followed by a rapid increase up to 100% RH. At low RH a significant number of the Br atoms are lost due to irradiation damage. With increasing humidity solvation increases ion mobility and gives rise to a partial recovery of the Br/K ratio. Above 60% RH the increase of the Br/K ratio accelerates. Above the deliquescence point (85% RH), the thickness of the water layer continues to increase and reaches more than three layers near saturation. The enhancement of the Br/K ratio at this stage is roughly a factor 2.3 on a 0.5 nm KBr film, indicating a strong preferential segregation of Br ions to the surface of the thin saline solution on SiO_2.

Keywords

Hydration, Ion segregation, Saline solution, Aerosol

Introduction

A drastic loss of ozone has been observed after the polar sunrise in the springtime Arctic troposphere. Previous reports have shown a concurrent increase of Br compounds (HOBr, Br_2, and BrO_x) in the atmosphere.[1] The source of Br is presumably sea salt, where it is present with a molar ratio relative to Cl of 1 to 660.[2] A considerable number of studies have been published on the mechanisms by which Br^- may react with ozone gas in the troposphere, leading to ozone depletion.[3-7] An important factor that amplifies the reaction of Br^- with ozone is the increased concentration of Br^- at the air- saline droplet interface. Various experiments[8-14] and simulations[15-18] on alkali halide solutions have demonstrated the propensity of large anions to segregate to the water-air interface. However, a large fraction of aerosols suspended in air are not pure alkali halide crystals but a mixture of dust particles from the deserts with salt crystals deposited on them as they are transported over oceanic regions.[19-22] While anion segregation at the air-liquid interface of pure saline solutions is now well established, the same phenomenon is not yet demonstrated for the case of thin films of saline solution on solid surfaces. The presence of an additional interface between the liquid and the solid interface may alter the segregation pattern because the ions can now partition between the two interfaces. This important information, which is missing today, is addressed in our study. In our approach we use SiO_2 films on Si wafers as a model substrate for dust particles, where Quartz is one of the dominant components. Indeed, a recent sum-frequency spectroscopy study has detected the presence of hydroxyl groups on both α-Quartz(0001) and amorphous SiO_2 surface by detection of the Si-OH stretch vibration mode.[23] Furthermore the vibrational spectrum of water/α-Quartz(0001) interface is qualitatively similar to that of water/amorphous SiO_2.[24] These results indicate that our amorphous SiO_2 layer can serve as a model for the Quartz surface found in sand.

Scanning polarization force microscopy (SPFM) is a powerful tool to study liquid surfaces as it can provide nanometer scale resolution images of surface topography, dielectric constant and surface potential simultaneously.[25-27] Several recent studies have been performed using this technique to study

salt/water interactions. SPFM observations of Br-doped NaCl have shown that Br-rich islands segregate to the surface after exposure to RH above 40% followed by drying, indicating the preferential solvation and segregation of Br^- ions.[28] In a recently published paper we used SPFM to show that on thin salt crystallites on SiO_2, the contact potential becomes negative for Br and Cl, but not for F upon adsorption of water and after deliquescence.[29] This phenomenon, interpreted as indication of the preferential anion segregation to the solution-air interface, is studied by spectroscopic means in this work.

We use ambient-pressure X-ray photoelectron spectroscopy (AP-XPS), which provides photoelectron spectra in the presence of water vapor up to several Torr.[30,31] Using this technique Ghosal et al.[32] have reported the enhancement of halide anions at the surface of saturated solutions of KBr and KI. More recently they have presented measurements of the ion distribution in mixed NaBr/NaCl aqueous solutions, showing the segregation of Br^- to the solution surface.[33] Here we use the same technique to study the concentration of Br^- at the surface of ~2.0 nm thick aqueous KBr solution films on SiO_2 films.

Experimental Section

Sample preparation. We used boron-doped p-type Si(100) wafers with a resistivity in the 0.02-0.05 Ω•cm range. The cleaning procedure was as follows: First the Si wafer samples were dipped into a solution of H_2SO_4 (95 – 97 wt%) : H_2O_2 (35 wt%)=3:1 (by volume) for 10 min to remove organic and metallic contamination. After rinsing with Millipore water for 1 min, they were dipped into a diluted HF solution (1 – 5 %) for 5 min to remove native oxide layers.[34] A clean oxide layer was formed by an ultraviolet ozone (UV/ozone) generator for 20 min.[35] After the UV/ozone treatment, the sample was immediately transferred to our AP-XPS chamber.

XPS experiments. XPS measurements were performed at beamline 11.0.2 of the Advanced Light Source (ALS), of the Lawrence Berkeley National Laboratory. The base pressure in the XPS chamber prior to the introduction of water vapor was $3x10^{-10}$ Torr. The sample was introduced into the chamber within 40 min after UV/ozone treatment. A thin KBr film was deposited on the SiO_2 surface from a solid KBr source, which was heated to 480 -520 °C. A differentially pumped electrostatic lens system separates the analysis chamber from the hemispherical photoelectron spectrometer.[30,31] We used water (ARISTAR® PLUS. HPLC, Low TOC Grade) from BDH, with a total organic carbon content less than 20 ppb. The water was degassed in three freeze-pump-thaw cycles. Water vapor was introduced up to a pressure of 1.5 Torr while the sample was cooled by a Peltier element.[36] In this manner we could obtain XPS spectra in the humidity range of 0 - 100 %.

Spectra of the Br3d, K2p, O1s, C1s and Si2p core levels were taken for incident photon energies of 275 eV, 490 eV, 735 eV, 490 eV and 309eV, respectively. These photon energies were chosen so that photoelectrons from these levels would have similar kinetic energies (~ 200 eV), thus ensuring the probing depth to be similar in all photoelectron spectra. A Br3d region was taken at photon energy of 475 eV in depth profile measurements. Photon energies of 275 eV and 490 eV were also used for Si2p spectra to calibrate binding energy scales. In all experiments the Br3d signal was collected first. The sample position was changed before acquisition of each Br3d spectrum in order to minimize X-ray beam damage, as described below.

When appropriate the spectra were normalized to photon flux, measured by a photodiode, synchrotron ring current, and photoemission cross sections[37]. Peak components of the spectra were deconvoluted using Gauss-Lorentz profiles after a Shirley background subtraction.

The thickness of the SiO_2 films on the Si substrate in our experiments was in the range from 1.7 to 2.1 nm, as calculated from the Si2p signal on a dry sample using the formula of Himpsel et al.[38] The formula is also applicable to estimate the thickness of adsorbed species on the Si sample, including carbon contamination, KBr and water.[39] We used 0.88 nm, 1.0 nm and 1.5 nm for the electron mean free

paths at the 200 eV kinetic energy through carbon contaminant,[40] KBr,[41] and water layers,[42] respectively. The estimated amount of carbon contamination on SiO_2 under dry condition was less than 0.1 monolayer (ML).

Results and Discussion

Water on KBr films

Figure 1 shows O1s XPS spectra from a KBr/SiO_2/Si sample in the presence of water vapor. The thickness of the KBr film under dry condition was 1.34 nm. The O1s region in includes contributions from oxygen in SiO_2, in the water film and in the gas phase.[43] Unfortunately the peaks from adsorbed water and from the oxide overlap strongly so that they can only be separated by deconvolution. To determine the contribution of each component the shape and the ratio of the O1s peak from SiO_2 to a normalized Si^{4+} component from a dry sample ($R = I_{\mathrm{O1s(oxide,\ dry)}}/I_{\mathrm{Si2p(Si4+,\ dry)}}$) were first obtained. Second, in the presence of water vapor, the contribution from SiO_2 ($I_{\mathrm{O1s(oxide)}}$) was estimated using the Si^{4+} peak in the Si2p spectrum ($I_{\mathrm{Si2p(Si4+)}}$) and R. The spectra were then fitted with three peaks as shown in Fig. 1(a). One is a contribution from SiO_2 ($I_{\mathrm{O1s(oxide)}}$) using the line shape determined under dry conditions. Another is from gas phase water. The remaining signal is assigned to adsorbed water and hydroxyls ($I_{\mathrm{O1s(water)}}$).

Figure 1(b) shows O1s XPS spectra as a function of RH. The spectra were acquired under a constant water vapor pressure of 1.5 Torr while the sample temperature was changed. All spectra are aligned using the SiO_2 peak (determined after deconvolution) as a reference. The arrows mark the positions assigned to the vapor and adsorbed water. As more water adsorbs the envelope of the compound peak shifts to the higher binding energy characteristic of molecularly adsorbed water. The absolute value of the gas phase peak shifts due to changes in work function of the sample.

By using formulae in the literature,[44] the thickness of water on SiO_2 prior to deposition of KBr films is given by:

$$d_{water} = \ell_{H_2O} \times Ln\left[\left\{1 - \exp\left(- d_{SiO_2} / \ell_{SiO_2}\right)\right\} \times \frac{I_{O1s(water)} n_{SiO_2} \sigma_{SiO_2} \ell_{SiO_2}}{I_{O1s(oxide)} n_{H_2O} \sigma_{H_2O} \ell_{H_2O}} + 1 \right] \quad (1)$$

When KBr films are present there is additional attenuation of the SiO_2 photoelectrons. The equation shown below is then used to obtain the thickness of water on a KBr/SiO_2 sample.

$$d_{water} = \ell_{H_2O} \times Ln\left[\left\{1 - \exp\left(- d_{SiO_2} / \ell_{SiO_2}\right)\right\} \times \exp\left(- d_{KBr} / \ell_{KBr}\right) \times \frac{I_{O1s(water)} n_{SiO_2} \sigma_{SiO_2} \ell_{SiO_2}}{I_{O1s(oxide)} n_{H_2O} \sigma_{H_2O} \ell_{H_2O}} + 1 \right] \quad (2)$$

The oxide and KBr thicknesses (d_{SiO_2} and d_{KBr}) were determined separately under dry conditions. The other parameters in eqs. (1) and (2) are listed in Table 1.

Figure 2(a) shows the water layer thickness obtained from the area of the O1s XPS spectra as a function of RH on four different samples. Open symbols represent data on a clean Si oxide without KBr films. The water layer thickness on the bare SiO_2 surface is less than in a previous report by about a factor of two,[43] especially in the low and medium RH regions. The discrepancy could originate from differences in sample preparation as it has been reported that the water layer thicknesses is quite sensitive to the surface pre-treatment, which determines the amount of hydroxyl groups on the surface and the degree of hydrophilicity of SiO_2.[45-47] The filled symbols in Fig. 2(a) represent data for KBr thin films of different thickness. It is apparent that more water layers are formed on samples with KBr films than on bare SiO_2 in the entire RH range. The water layer thickness increases rapidly up to approximately 0.3 nm, (one monolayer assuming 0.3 nm per layer) until approximately 30% RH (Region I). This agrees well with our previous SPFM results, in which a water layer covers both KBr crystallites and SiO_2 substrate at ~30% RH.[29] After this a plateau is observed until 60% RH (Region II). When alkali-halide crystal surfaces are exposed to water vapor, there is a critical RH value below which ions at steps solvate preferentially and become mobile. Above this critical RH value, ionic solvation

occurs over the entire surface. This critical RH is 55% in the case of KBr single crystals,[27] and might correspond to the boundary between Region II and III. Above 60% RH, the water layer thickness increases rapidly, reaching more than three layers above 90% RH. This growth behavior coincides with that on bulk alkali halide crystals, as reported previously.[48-50] The boundary between Regions III and IV has been drawn at the nominal deliquescence point of KBr (85% RH).[27] Figure 2(b) shows a more detailed uptake curve above 80% RH for a 0.49 nm thick KBr film.

Radiation damage

Beam damage by the X-ray beam from the synchrotron is an unwelcome but hardly avoidable part of the experiments. Ionic compounds are particularly sensitive due to ionization of anions leading to their facile emission from the surface. We thus performed a study of the irradiation effects on our samples. Figure 3 shows the measured counts, normalized by the synchrotron ring current, from the emitted Br3d photoelectrons as a function of exposure time to a beam of 275 eV X-rays. The flux density was $1.9\times10^{13} - 2.8\times10^{13}$ photons/sec in an irradiated area of 7.1×10^{4} μm^2. The thickness of the deposited KBr film was approximately 0.2 nm. We used a pass energy of 20 eV in order to broaden the spectral energy window to ~5 eV. This enabled us to measure the peak area of Br3d continuously after the start of the X-ray irradiation, without any influence of small energy shifts of the peak. The data at 25%, 75% and 95% RH were obtained at a constant water vapor pressure of 1.5 Torr. The data at 0% RH were obtained at 1.5×10^{-6} Torr. Longer exposure to the X-ray beam results in a decreasing count rate at 0%, 75% and 95% RH, showing that substantial damage results in a loss of Br. At 25% RH, the count rate remains at a constant and comparatively low value for 60 seconds.

The loss of Br atoms at 0% RH is not surprising as it has been known since 1930 that X-ray irradiation creates defects, such as anion vacancies, interstitials and color centers in alkali halides.[51-54] The substantially lower Br signal at 25% RH observed already in the first data point in Fig. 3 indicates

that a fast initial loss of Br takes place within the first second of irradiation. This additional damage must be due to photochemical reactions involving water molecules. Soft X-ray photons can indeed decompose water molecules in the surface layer or in the vapor phase to create radicals such as hydroxyl OH, atomic oxygen O, and hydroperoxyl OH_2.[55,56] Once OH radicals are formed, they can oxidize aqueous Br^- to form molecular Br_2,[57-60] which desorbs from the sample. Another experiment at 50% RH (not shown) showed a similar trend. Beam damage occurs still at 75% RH, although the amount of Br lost is smaller. At 95% RH the initial fast damage part is further reduced, although after prolonged exposure a substantial amount of Br loss is again observed.

The apparently lower loss of Br at higher humidity values is probably related to the increased mobility of solvated Br^-, which partially refills the irradiated spot by diffusing from the surrounding areas, as will be discussed in detail later. Beam damage was found to be negligible for the K2p, O1s, C1s and Si2p spectra.

Atomic concentration ratio of Br to K

Figure 4 shows the Br/K ratio determined from the peak areas as a function of RH. Open symbols represent data on a cleaved KBr bulk single crystal. The Br/K ratio is found to be between 0.6 and 0.7 up to ~85% RH, a value that is lower than the stoichiometric ratio of 1.0. Similar experiments using bulk crystals reported an average ratio of about 0.85 (for RHs below the deliquescence point), closer to the stoichiometric ratio.[32] A possible explanation for the larger deviations from the expected value in the present experiments is a higher loss of Br atoms due to more intense beam damage. A second possibility is uncertainties in measured photon fluxes which are used to normalize the Br3d ($h\nu$ = 275 eV) and K2p ($h\nu$ = 490 eV) spectra.

In all three KBr films referred to in Fig. 4(a), the initial Br/K ratios at 0% RH are 0.3 – 0.4, about half the 0.7 value for the single crystal. A possible explanation for the difference lies in the thin nature of the

salt film, up to 5 layers approximately. This makes the percentage of Br lost in the analyzed region larger than in the bulk crystal, where undamaged deeper layers contribute to the signal. As can be seen in the figure, the Br/K ratio drops rapidly on the submonolayer KBr films (0.15 nm and 0.18 nm) in Region I (0% - 30% RH). This is due to additional beam damage in the presence of water vapor discussed in the previous section. For the thicker KBr film (1.34 nm) the Br/K ratio decreases more slowly. In all cases however, above 60% RH there is a rapid recovery of the Br signal, which, as described above, is probably related to Br replenishment by diffusion from the surroundings.

At 85% RH, the deliquescence point of KBr, the bulk crystal dissolves and the Br/K ratio increases abruptly, indicating Br segregation to the droplet surface.[32] Figure 4(b) shows in more detail the evolution of the Br/K ratio for a 0.49 nm KBr film above 80% RH. In this example the ratio increases smoothly rather than abruptly, from approximately 0.25 at 80% RH to 0.92 at 99% RH.

The increase of the Br/K ratio to values close to 1 in spite of the substantial loss due to beam damage supports a model where, as the liquid film grows in thickness, the K^+ ions stay close to the substrate while Br concentrates at the liquid-gas interface. Let us assume for simplicity a complete separation of ions in the liquid film, with Br^- ions present only at the liquid/vapor interface, and K^+ at the liquid-SiO_2 interface. From Fig. 2(b), we see that the water layer thickness increases from 0.6 nm (90% RH) to 2.1 nm (near saturation). This should attenuate the intensity of K2p $\left(I_K^0\right)$ so that the detected intensity $\left(I_K\right)$ becomes:

$$I_K = I_K^0 \times e^{-\frac{d_{solution}}{\ell_{solution}}}, \qquad (3)$$

where $d_{solution}$ and $\ell_{solution}$ are the solution thickness and electron mean free path in the solution, respectively. Assuming that the intensity of Br3d $\left(I_{Br}\right)$ does not change, using $\ell_{solution}$ = 1.5 nm in Eq. (3), we obtain an increase in the Br/K ratio $\left(I_{Br}/I_K\right)$ of a factor of 2.7 from 90% RH to near saturation, a value that is close to the one (2.3) we obtain from Fig. 4(b).

When the RH reached 100% and water droplets became macroscopically visible, the Br and K signals were too weak to be detected, as both Br^- and K^+ become diluted to below the detection limit of XPS.

Analysis of the K2p and Br3d peaks

Figure 5 shows the K2p and Br3d XPS regions for a 0.15 nm thick film on SiO_2 at selected RH values. The binding energy was calibrated in the following manner. First, Si2p spectra were recorded at photon energies of 490 eV and 275 eV at each RH, right after each Br3d or K2p spectra. All Si2p spectra were deconvoluted into Si^0, Si^{1+}, Si^{2+}, Si^{3+} and Si^{4+} components.[38] Second, the binding energy of Si2p at 0% RH was calibrated using the known values for elemental Si (99.4 eV). The peak position of the Si^{4+} component at 0% RH was in this way determined to be 103.5 eV. The binding energies scale at each RH were then adjusted so that the Si^{4+} component was equal to 103.5 eV.

As shown in the left column in Fig. 5, each K2p spectrum can be fit with a single p-orbital doublet. The binding energy monotonically shifts to a lower value as RH increases: -0.07 eV at 8% RH, -0.29 eV at 62% RH, and -0.45 eV at 95% RH. The Br3d spectra in the right column in Fig. 5 show the main peak of the d-orbital doublet at 69.2 eV, which remains constant for all RH values. The evaluation of absolute binding energies is not straightforward since the low electrical conductance of the KBr film[50] and the SiO_2 substrate leads to charging of the surface. The amount of charging depends on the photon flux and the total photoemission cross section, quantities that are photon energy dependent. Besides the unwanted shifts due to charging, the K2p and Br3d binding energies can also change due to hydration of cations (K^+) and anions (Br^-), i.e. true chemical shifts, as shown by previous studies.[61-64]

The data in Fig. 5 show that above 29% RH, a change in the shape of the Br peaks takes place in the high binding energy side, which becomes more noticeable as the RH continues to increase. In order to fit these spectra additional peaks are needed, as indicated by the blue curve. The binding energy of the new doublet is 70.1 eV, whereas that of the dominant peak is 69.2 eV. The area ratio of the additional peak to the dominant peak at 95% RH is 0.34, three times higher than that at 62% RH (0.11). This additional Br3d peak indicates that two different chemical surroundings exist for Br^- at high humidity. Recalling the preferential segregation of anions to the water surface at high RH described in the previous section, the most straightforward explanation for the additional peak is the presence of a surface and a bulk Br^- species. Figure 6 shows spectra acquired at different photon energies at 90% RH. The thickness of the KBr film in this example was 0.56 nm. A lower photon energy generates photoelectrons with lower kinetic energies, which gives more surface-sensitive information. The area ratio of the additional peak to

the dominant peak in Fig. 6(a) is 0.22, approximately twice as high than that in Fig. 6(b) (0.12). This suggests that the Br species giving rise to the additional doublet peak at higher binding energy are localized at the solution surface. No such peak doubling is observed for the K cation, in line with a model where only the anions segregate preferentially to the liquid-vapor interface.

The chemical state of the new Br species is unknown at present. Several models, including different solvation shell configurations for the surface and bulk species can be considered. It is clear however, that the shift to higher binding energy is contrary to the expectation of the simple model where the positive end of the water dipole points to the Br^- ion, which should shift the peak to lower binding energy. Others models including the presence of surface contaminants binding to the surface Br, or modifying its solvation structure need to be considered. This is currently being investigated.[65]

Conclusions

We have studied the growth of water layers on KBr thin films on SiO_2 using ambient pressure X-ray photoelectron spectroscopy. The water layers formed as the RH increases are always thicker than those formed on the bare SiO_2 surface.

We have documented the substantial damage induced by X-ray irradiation, and we have shown that this damage is more severe in the presence of water, indicative of photochemical reactions leading to the loss of Br. These reactions occur within 1 second of irradiation. At high RH, the increasing mobility of solvated ions partly replenishes the irradiated area by diffusion of Br ions from surrounding regions.

In spite of the loss of Br due to beam damage, the ratio of Br/K increases beyond that of the original film, indicative of preferential anion segregation at the surface of the solution. Interestingly, and unlike in bulk crystals, in the thin films the ratio increases smoothly rather than abruptly beyond the deliquescence point.

We have shown that the K2p spectra can be fit with a single p-orbital doublet peak in the entire RH. On the other hand, a Br3d spectrum requires an additional d-orbital doublet peak above 60% RH, with a binding energy higher than that of the dominant peak. This additional peak is more noticeable at

higher RH. A depth profile measurement indicated that the additional peak derives from Br atoms segregated to the water surface.

The present results are relevant to the atmospheric chemistry of dust particles, like those formed in deserts and traveling over oceans, which then become covered by salt deposits. Our work shows that the previously reported segregation of anions at the vapor-liquid interface is also occurring in the very thin solution films formed at high humidity, where another interface –the liquid-solid interface is present at nanometer distances.

Acknowledgement

The authors would like to thank Dr. Albert Verdaguer for technical discussions on AP-XPS. This work was supported by the Director, Office of Science, Office of Basic Energy Sciences, Materials Sciences and Engineering Division, of the U.S. Department of Energy under Contract No. DE-AC02-05CH11231. K.A. acknowledges financial support from Yamada Science Foundation.

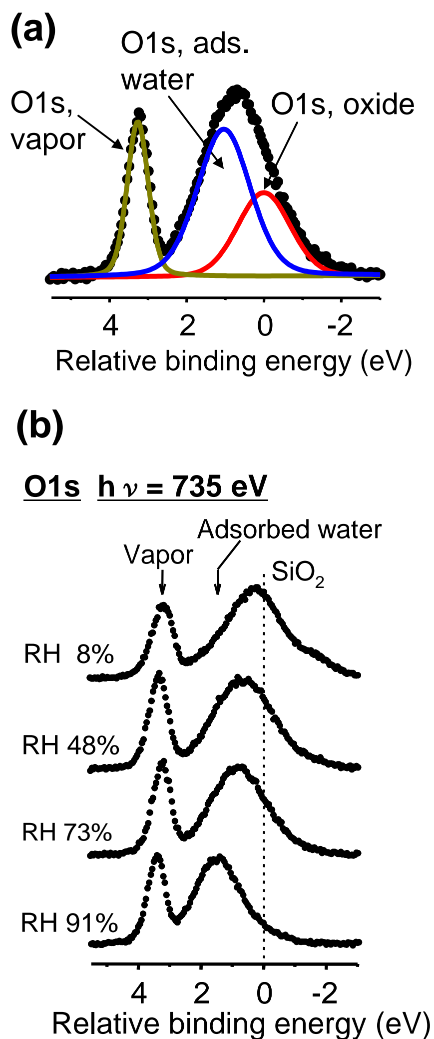

Figure 1. O1s XPS spectra from a 1.34 nm KBr film on a SiO_2/Si sample in the presence of 1.5 Torr of water vapor. (a) Deconvolution of the spectra by fitting to three peaks, shown in red, blue and yellow. These correspond to O from SiO_2, from adsorbed water and from gas phase water, respectively. The peak areas obtained from O in SiO_2 ($I_{O1s(oxide)}$, red curve) and from O in the adsorbed water layer ($I_{O1s(water)}$, blue curve) were used to obtain the thickness of the water layers. (b) Spectra at selected RH values. The energy scale is referenced to the O peak from SiO_2 (see text).

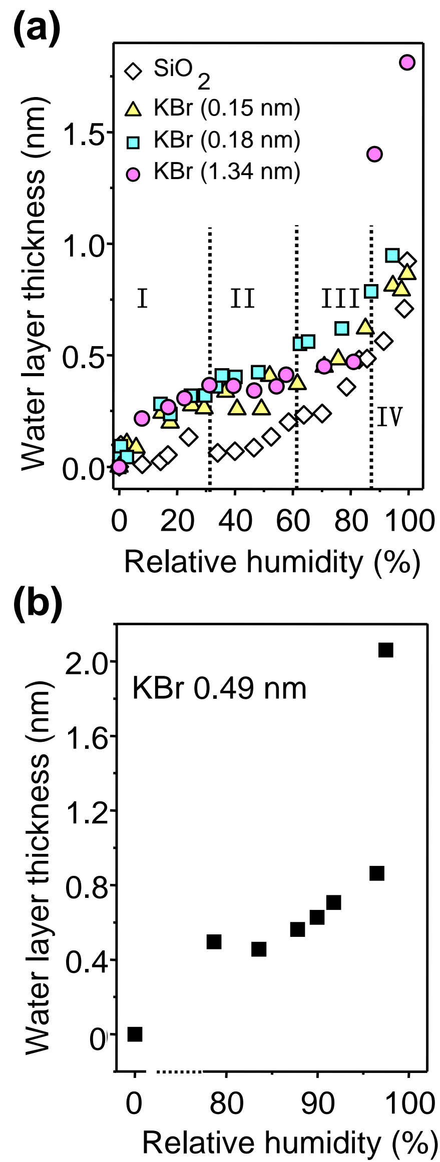

Figure 2. (a) Water layer thickness as a function of RH. Various regions (I-IV) are marked and discussed in the text. (b) Detailed water thickness evolution in the RH range from 80% to near saturation.

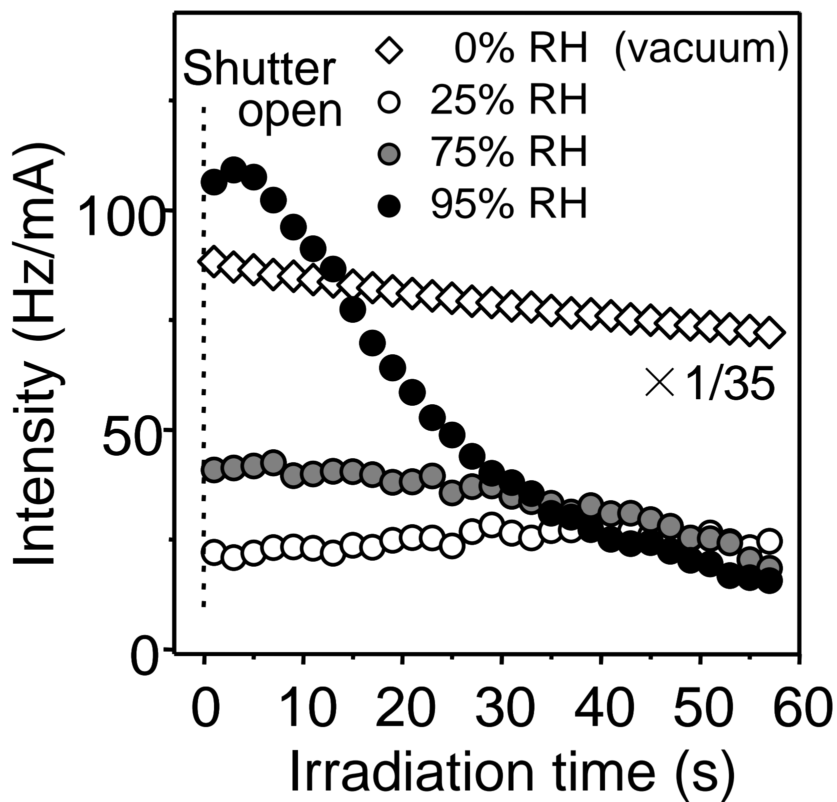

Figure 3. Intensity of Br3d as a function of exposure time to the X-ray beam. The measured counts were normalized by the ring current. Data points were acquired every two seconds. Notice the large increase in the initial damage (occurring before measurement of the first point) at 25% RH at a constant water vapor pressure of 1.5 Torr.

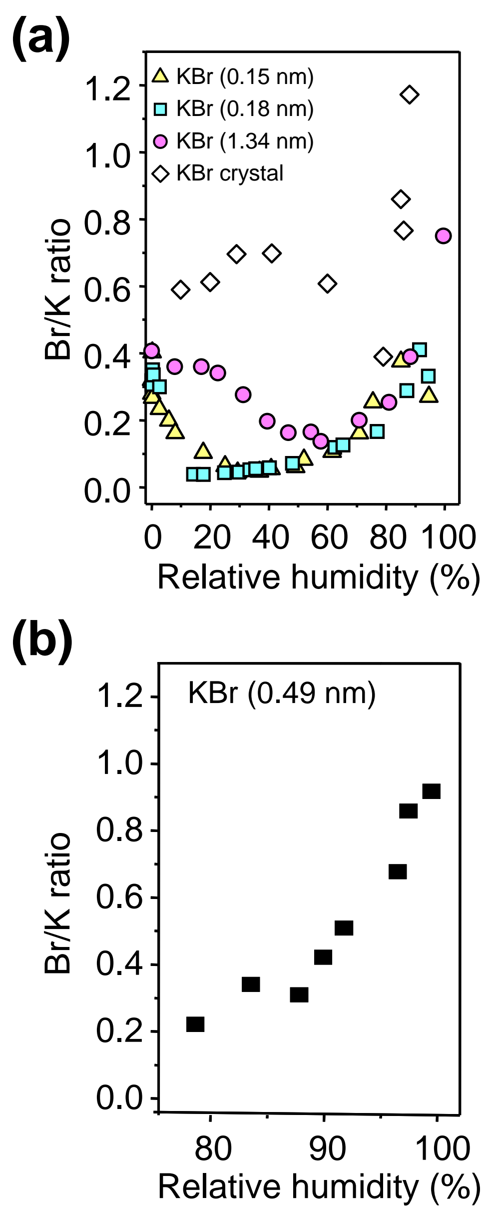

Figure 4. (a) Br/K ratio as a function of RH. (b) Detailed Br/K ratio in the RH range from 80% to near saturation (~99%RH).

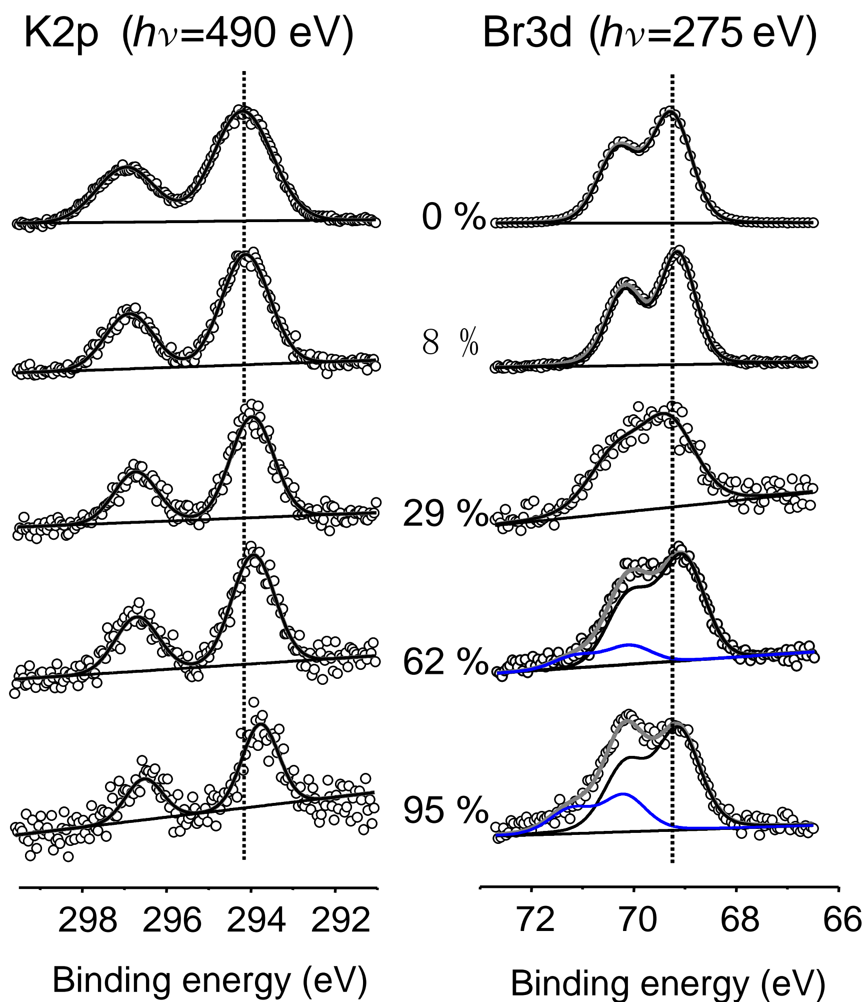

Figure 5. K2p and Br3d spectral regions from a 0.15 nm KBr film on SiO_2 at selected RH values. Broken lines indicate the positions of $K2p_{3/2}$ and $Br3d_{5/2}$ peaks at 0% RH. For K2p, the binding energy monotonically shifts to a lower value as RH increases. For Br3d, the shift in the binding energy of a main peak is smaller than that in the case of K2p. Instead, an additional doublet peaks is needed to fit the spectrum, as indicated by blue curves above 62% RH.

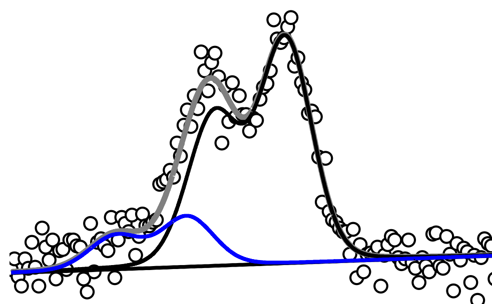

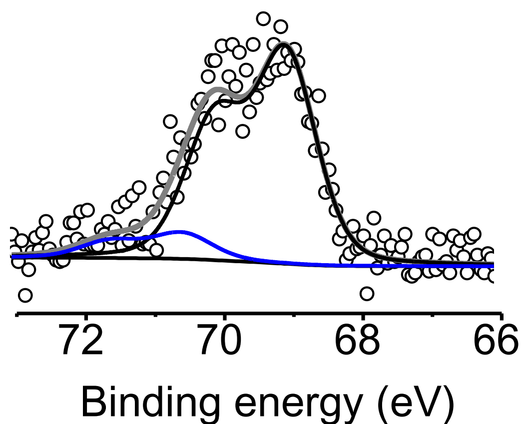

Figure 6. Spectra from Br3d from a 0.56 nm film at 90% RH at two different photon energies: (a) $h\nu$ = 275 eV, (b) $h\nu$ = 475 eV, to discriminate surface and bulk contributions.

Table 1. Parameters for calculating the thickness of water layers. n, σ, and ℓ are the atomic density of oxygen atoms, the atomic photoionization cross-section of oxygen, and the electron mean free path at the 200 eV kinetic energy, respectively.

	n ($10^{22}/cm^3$)	σ (Mb)	ℓ (nm)
SiO_2	4.56	0.25	1.0
H_2O	3.35	0.25	1.5
KBr	-	-	1.0

References

1. Impey, G. A.; Mihele, C. M.; Anlauf, K. G.; Barrie, L. A.; Hastie, D. R.; Shepson, P. B. *J. Atmos. Chem.* **1999**, *34*, 21.

2. Lide, D.R. Handbook of Chemistry and Physics; CRC Press: Florida, 2008-2009.

3. Barrie, L.A.; Bottenheim, J. W.; Schnell, R. C.; Crutzen, P. J.; Rasmussen, R. A. *Nature* **1988**, *334*, 138.

4. Finlayson-Pitts, B. J.; Livingston, F. E.; Berko, H. N. *Nature* **1990**, *343*, 622.

5. McConnell, J. C.; Henderson, G. S.; Barrie, L.; Bottenheim, J.; Niki, H.; Langford, C. H.; Templeton, E. M. J. *Nature* **1992**, *355*, 150.

6. Impey, G. A.; Shepson, P. B.; Hastie, D. R.; Barrie, L. A.; Anlauf, K. G. *J. Geophys. Res. D* **1997**, *102*, 16005.

7. Foster, K. L.; Plastridge, R. A.; Bottenheim, J. W.; Shepson, P. B.; Finlayson-Pitts, B. J.; Spicer, C. W. *Science* **2001**, *291*, 471.

8. Zangmeister, C. D.; Turner, J. A.; Pemberton, J. E. *Geophys. Res. Lett*. **2001**, *28*, 995.

9. Petersen, P. B.; Saykally, R. J. *J. Phys. Chem. B* **2006**, *110*, 14060.

10. Petersen, P. B.; Saykally, R. J. *Annu. Rev. Phys. Chem*. **2006**, *57*, 333.

11. Liu, D.; Ma, G.; Levering, L. M.; Allen, H. C. *J. Phys. Chem. B* **2004**, *108*, 2252.

12. Mucha, M; Frigato, T.; Levering, L. M.; Allen, H. C.; Tobias, D. J.; Dang, L. X.; Jungwirth, P. *J. Phys. Chem. B* **2005**, *109*, 7617.

13. Ishiyama, T; Morita, A. *J. Phys. Chem. C* **2007**, *111*, 738.

14. Grieves, G. A.; Petrik, N.; Herring-Captain, J; Olanrewaju, B.; Aleksandrov, A.; Tonkyn, R. G.; Barlow, S. A.; Kimmel, G. A.; Orlando, T. M. *J. Phys. Chem. C* **2008**, *112*, 8359.

15. Jungwirth, P; Tobias, D. J. *J. Phys. Chem. B* **2001**, *105*, 10468.

16. Jungwirth, P; Tobias, D. J. *J. Phys. Chem. B* **2002**, *106*, 6361.

17. Eggimann, B. L.; Siepmann, J. I. *J. Phys. Chem. C* **2008**, *112*, 210.

18. Levin, Y.; dos Santos, A. P.; Diehl, A. *Phys. Rev. Lett.* **2009**, *103*, 257802.

19. Andreae, M. O.; Charlson, R. J.; Bruynseels, F.; Storms, H.; Van Grieken, R.; Maenhaut W. *Science* **1986** ,*232*, 1620.

20. Fan, X-B.; Okada, K.; Niimura, N.; Kai, K.; Arao, K.; Shi, G-Y.; Qin, Y.; Mitsuta Y. *Atmos. Env*. **1996**, *30*, 347.

21. VanCuren, R. A. *J. Geophys. Res. D* **2003**, *108*, 4623.

22. Levin, Z.; Teller, A.; Ganor, E.; Yin, Y. *J. Geophys. Res*. *D* **2005**, *110*, D20202.

23. Liu, W-T.; Shen, Y. R. *Phys. Rev. Lett*. **2008**, *101*, 016101.

24. Ostroverkhov, V.; Waychunas, G. A.; Shen, Y. R. *Chem. Phys. Lett*. **2004**, *386*, 144.

25. Hu, J.; Xiao, X-D.; Ogletree, D. F.; Salmeron, M. *Science* **1995**, *268*, 267.

26. Salmeron, M; Xu, L.; Hu, J.; Dai, Q. *MRS Bull*. **1997**, *8*, 36.

27. Luna, M.; Rieutord, F.; Melman, N. A.; Dai, Q.; Salmeron, M. *J. Phys. Chem. A* **1998**, *102*, 6793.

28. Ghosal, S.; Verdaguer, A.; Hemminger, J. C.; Salmeron, M. *J. Phys. Chem. A* **2005**, *109*, 4744.

29. Arima, K.; Jiang, P.; Lin, D-S.; Verdaguer, A.; Salmeron, M. *J. Phys. Chem. A* **2009**, *113*, 9715.

30. Ogletree, D. F.; Bluhm, H.; Lebedev, G.; Fadley. C. S.; Hussain, Z; Salmeron, M. *Rev. Sci. Instrum*. **2002**, *73*, 3872.

31. Salmeron, M.; Schlögl, R. *Surf. Sci. Rep*. **2008**, *63*, 169.

32. Ghosal, S.; Hemminger, J. C.; Bluhm, H.; Mun, B. S.; Hebenstreit, E. L. D.; Ketteler, G.; Ogletree, D. F.; Requejo, F. G.; Salmeron, M. *Science* **2005**, *307*, 563.

33. Ghosal, S.; Brown, M. A.; Bluhm, H; Krisch, M. J.; Salmeron, M.; Jungwirth, P.; Hemminger, J. C. *J. Phys. Chem. A* **2008**, *112*, 12378.

34. Arima, K.; Endo, K.; Kataoka, T.; Oshikane, Y.; Inoue, H.; Mori, Y. *Appl. Phys. Lett.* **2000**, *76*, 463.

35. Takahagi, T.; Nagai, I.; Ishitani, A.; Kuroda, H.; Nagasawa, Y. *J. Appl. Phys*. **1988**, *64*, 3516.

[36.] Ogletree, D. F.; Bluhm, H.; Hebenstreit, E. B.; Salmeron, M. *Nucl. Instrum. Meth. in Phys. Res. A* **2009**, *601*, 151.

[37.] Yeh, J. J.; Lindau, I. *Atomic Data Nucl. Data Tables* **1985**, *32*, 1.

[38.] Himpsel, F. J.; McFeely, F. R.; Taleb-Ibrahimi, A.; Yarmoff, J. A.; Hollinger, G. *Phys. Rev. B* **1988**, *38*, 6084.

[39.] Seah, M. P.; Spencer, S. J. *J. Vac. Sci. Technol. A* **2003**, *21*, 345.

[40.] Tanuma, S.; Powell, C. J.; Penn, D. R. *Surf. Interface Anal.***1991**, *17*, 911.

[41.] Akkerman, A.; Boutboul, T.; Breskin, A.; Chechik, R.; Gibrekhterman, A.; Lifshitz, Y. *Phys. Stat. Sol. b* **1996**, *198*, 769.

[42.] The mean free path of water was calculated using the software of NIST ELECTRON INELASTIC-MEAN-FREE-PATH DATABASE by National Institute of Standards and Technology, USA.

[43.] Verdaguer, A.; Weis, C.; Oncins, G.; Ketteler, G.; Bluhm, H.; Salmeron, M. *Langmuir* **2007**, *23*, 9699.

[44.] Deng, X.; Herranz, T.; Weis, C.; Bluhm, H.; Salmeron, M. *J. Phys. Chem. C* **2008**, *112*, 9668.

[45.] Sumner, A. L.; Menke, E. J.; Dubowski, Y.; Newberg, J. T.; Penner, R. M.; Hemminger, J. C.; Wingen, L. M.; Brauers, T.; Finlayson-Pitts, B. J. *Phys. Chem. Chem. Phys*. **2004**, *6*, 604.

[46.] Asay, D. B.; Kim, S. H. *J. Phys. Chem. B* **2005**, *109*, 16760.

[47.] Tero, R. *Phys. Chem. Chem. Phys*. **2006**, *8*, 3885.

[48.] Peters, S. J.; Ewing, G. E.; *Langmuir* **1997**, *13*, 6345.

[49.] Foster, M. C.; Ewing, G. E.; *J. Chem. Phys*. **2000**, *112*, 6817.

[50.] Verdaguer, A.; Segura, J. J.; Fraxedas, J.; Bluhm, H.; Salmeron, M. *J. Phys. Chem. C* **2008**, *112*, 16898.

[51.] Seitz, F. *Rev. Mod. Phys.* **1946**, *18*, 384.

[52.] Hersh, H. N. *Phys. Rev*. **1966**, *148*, 928.

[53.] Itoh, N.; Tanimura, K. *J. Phys. Chem. Solids* **1990**, *51*, 717.

[54] Thomas III, J. H. *Beam Effects, Surface Topography, and Depth Profiling in Surface Analysis; Chapter 1*. Edited by A. W. Czanderna, T. E. Madey and C. J. Powell. Plenum Publishing Corporation. New York, 1998.

[55] Henderson, M. A. *Surf. Sci. Rep.* **2002**, *46*, 1.

[56] Laffon, C.; Lacombe, S.; Bournel, F.; Parent, Ph. *J. Chem. Phys*. **2006**, *125*, 204714.

[57] Mamou, A.; Rabani, J.; Behar, D. *J. Phys. Chem*. **1977**, *81*, 1447.

[58] Mozurkewich, M. *J. Geophys. Res*. **1995**, *100*, 14199.

[59] Anastasio, C. ; Mozurkewich, M. *J. Atmos. Chem*. **2002**, *41*, 135.

[60] Thomas, J. L.; Jimenez-Aranda, A. ; Finlayson-Pitts, B. J. ; Dabdub, D. *J. Phys. Chem. A* **2006**, *110*, 1859.

[61] Siegbahn, H. *J. Phys. Chem.* **1985**, *89*, 897.

[62] Winter, B.; Faubel, M. *Chem. Rev*. **2006**, *106*, 1176.

[63]. Weber, R.; Winter, B.; Schmidt, P. M.; Widdra, W.; Hertel, I. V.; Dittmar, M.; Faubel, M. *J. Phys. Chem. B* **2004**, *108*, 4729.

[64] Winter, B.; Weber, R.; Hertel, I. V.; Faubel, M.; Jungwirth, P.; Brown, E. C.; Bradforth, S. E. *J. Am. Chem. Soc*. **2005**, *127*, 7203.

[65] Brown, M.A.; Krisch, M.K.; Arima, K.; Bluhm, H.; Salmeron, M.; Hemminger, J.C.; unpublished.

LEGAL DISCLAIMER

This document was prepared as an account of work sponsored by the United States Government. While this document is believed to contain correct information, neither the United States Government nor any agency thereof, nor The Regents of the University of California, nor any of their employees, makes any warranty, express or implied, or assumes any legal responsibility for the accuracy, completeness, or usefulness of any information, apparatus, product, or process disclosed, or represents that its use would not infringe privately owned rights. Reference herein to any specific commercial product, process, or service by its trade name, trademark, manufacturer, or otherwise, does not necessarily constitute or imply its endorsement, recommendation, or favoring by the United States Government or any agency thereof, or The Regents of the University of California. The views and opinions of authors expressed herein do not necessarily state or reflect those of the United States Government or any agency thereof or The Regents of the University of California.